Anionic and cationic redox and interfaces in batteries: advances from soft X-ray absorption spectroscopy to resonant inelastic scattering

Wanli Yang[a*], *Thomas P. Devereaux*[bc*]

[a]Advanced Light Source, Lawrence Berkeley National Laboratory, One cyclotron road, Berkeley, CA 94720 USA

[b]Stanford Institute for Materials and Energy Sciences, SLAC National Accelerator Laboratory and Stanford University, Menlo Park, CA 94025, USA.

[c]Geballe Laboratory for Advanced Materials, Stanford University, Stanford, CA 94305, USA.

*Corresponding Authors: WLYang@lbl.gov (WY), tpd@stanford.edu (TPD)

Graphic Abstract:

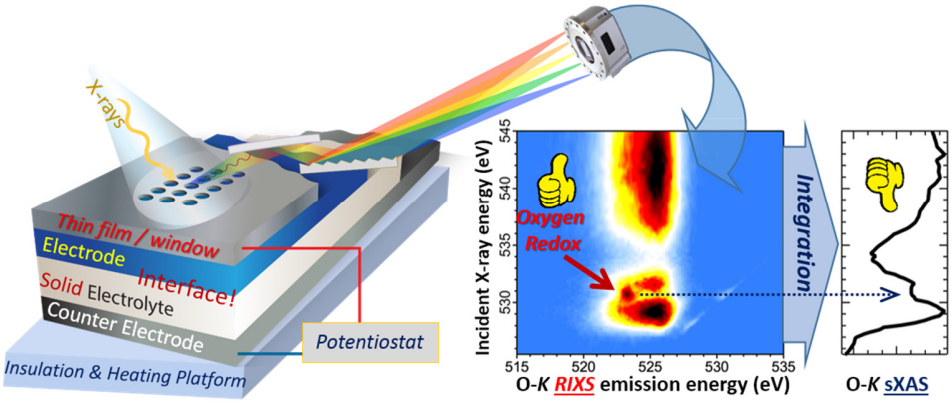

ABSTRACT

Recent advances in solid-state batteries (SSBs) have triggered both the challenges and opportunities on studying the materials and interfaces in batteries. Here, we review the recent developments and employments of soft X-ray spectroscopy for studying the interfaces and electrode materials. The focus of this review is on the recently realized mapping of resonant inelastic X-ray scattering (mRIXS), which is demonstrated to be a powerful probe of battery chemistry with superior sensitivity. Six different channels of soft X-ray absorption spectroscopy (sXAS) are introduced and summarized for different purposes. Although conventional sXAS remains an effective tool for quantitative analysis of the transition-metal states and surface chemistry, we elaborate the limitations of sXAS with experimental results and conclude that sXAS is unreliable for studying oxygen redox reactions. We then present the mRIXS as the tool-of-choice for fingerprinting oxygen redox and summarize several crucial observations. We conclude that the interpretation of the mRIXS feature will reveal the true fundamental and universal nature of oxygen redox in various battery electrodes, a direction that the field should pay attention and follow. The combination of these advanced soft X-ray techniques will contribute unprecedented information for characterizing interfaces and high-performance electrodes with novel redox couples.

Keywards: Soft X-ray Spectroscopy; Battery; Anionic Redox; Resonant Inelastic X-ray Scattering; Soft X-ray Absorption Spectroscopy; Surface and Interface

1. Introduction

Developing advanced battery systems for electric energy storage has been a pressing demand for today's sustainable energy applications such as the electric vehicles and green power grid. However, the dilemma of the competing parameters in batteries, especially between the energy density and safety, has so far hindered the successful commercialization of many innovations on high-performance battery materials and concepts. Under this circumstance, all solid-state batteries (SSBs) have recently attracted much attention due to their inherent safety and stability in comparison with conventional liquid electrolyte [1-3], which could potentially enable the employments of high energy and power density battery electrodes, particularly Lithium metal anode [2, 4-6]. Although several industry entities have now been established based on SSBs, technical challenges remain formidable for further optimizing SSBs into a revolutionary energy storage system to truly replace batteries based on conventional liquid electrolyte.

Besides the optimization of the intrinsic ion conductivity of solid-state electrolytes [7], SSBs often suffer unfavorable interface problems at the electrolyte domain boundaries and at the electrode-electrolyte interface [7-9]. Detecting and understanding the electrode-electrolyte and intra-electrolyte interfaces are critical for the development of SSBs. For example, the interface has been recognized as one of the key challenges for the practical applications of metal anodes in various systems [2]. Unfortunately, the chemical environment at the interface is in the approximation to the bulk electrode/electrolyte materials. Other than the structural probes through microscopy [10], direct measurements of the chemical and physical properties at the interface require incisive tools with superior

chemical sensitivity, so that the subtle but crucial effect of the interface could be resolved in experiments.

On the other hand, a high-performance positive electrode is also highly desirable to provide a balanced system in terms of energy and power density, which remains a bottleneck in typical battery systems. Developments of high energy and power density cathodes have been progressing very slowly, but conceptual breakthroughs on introducing novel redox couples, especially oxygen redox in oxide electrodes, have recently revitalized the field [11]. Indeed, if anionic redox could be realized in a highly reversible way, it could provide the promised energy and power density in battery cathodes to enable the ultimate SSB system with balanced electrodes. Additionally, other unusual chemical states of transition metals (TMs) could also be produced through the electrochemical process in batteries, especially atypically high valence states, e.g., Fe^{4+}, which also hold the promise to achieve improved capacity in cathodes. For such novel redox couples, a reliable detection is a nontrivial issue, which is partially the reason why such topics are often under active debate in both practical applications and fundamental understandings. For example, the anionic redox in oxide cathodes has been proposed to originate from peroxo-like oxygen dimers [12-16], oxygen holes that are localized [17, 18], or enabled by some specific structural and chemical configurations [19-21]. In addition to the debates on the fundamental mechanism, there has been no reliable quantification of the oxygen redox in battery electrodes, which is directly related with the practical issue on reversibility. Although the seemingly elemental-sensitive soft X-ray spectroscopies, especially X-ray photoelectron spectroscopy (XPS) and sXAS have been extensively employed, they fail to deliver reliable information on the intrinsic bulk oxygen chemistry, as elaborated in the

discussions below. Again, incisive tools beyond conventional spectroscopy are keenly required for a reliable characterization of the novel redox couple involved in bulk electrodes.

This review covers recent demonstrations of core-level photon-in-phonon-out (PIPO) soft X-ray spectroscopy (SXS) in the methodology, analysis, and technical innovations dedicated for studying battery materials. Because conventional sXAS for battery interface and electrode studies has been reviewed before [22-24], here we focus on the recent developments and demonstrations, especially the mapping of resonant inelastic X-ray scattering (mRIXS). We first introduce various kinds of PIPO SXS with emphasis on mRIXS. We then show representative examples on studying battery materials in i) surfaces and interfaces, ii) TM cationic redox couple, and iii) anionic redox couples. We show examples of both sXAS and RIXS examples for each section. Particularly for the oxygen redox studies, experimental data of O-*K* sXAS of olivine and spinel electrodes are presented to show that neither the intensity nor the lineshape of sXAS is a reliable probe of oxygen redox. We show that a specific mRIXS feature fingerprints the bulk oxygen redox. A universal mechanism is indicated for both *3d* and *4d* TM oxides by mRIXS results, and it is clear that the ultimate understanding of oxygen redox mechanism has to be associated with the specific mRIXS feature. At the end, we provide our perspectives on utilizing the advanced SXS for SSB researches. SSB naturally enable the *in-situ/operando* SXS experiments, which provides unique opportunities for studying the interfaces and the anionic/cationic redox couples in real-world batteries.

2. PIPO SXS techniques and RIXS

2.1 Fundamental Excitation and Decay Channels in SXS

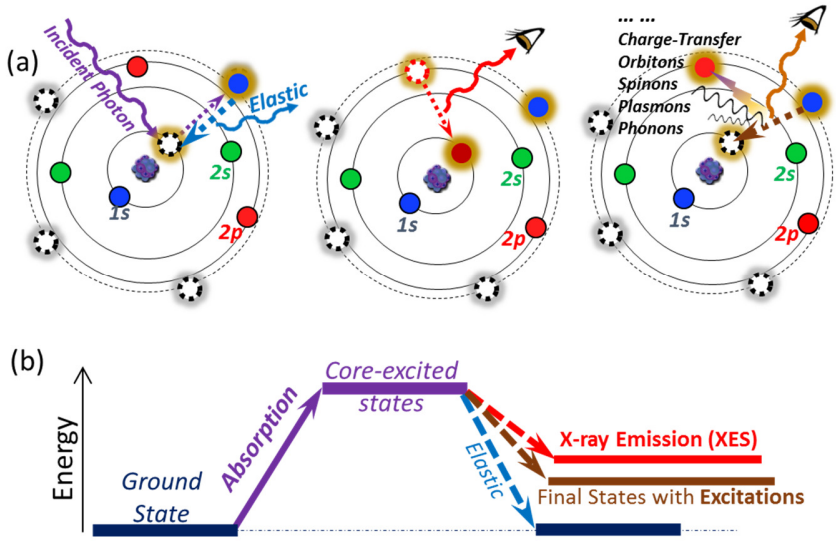

Fig. 1 Schematic of PIPO SXS. (a) is the simplified atomic models of sXAS (left), XES (middle), and RIXS (right). (b) displays the different states involved in the RIXS process upon energy scale (vertical).

The emission of photons through soft X-ray PIPO techniques is triggered by a core electron excitation by a tunable incident X-ray, i.e., the X-ray absorption process (Fig. 1a). Note "sXAS" is used in this work to differentiate it from hard X-ray "XAS", which is significantly different in many aspects [22]. The excited states will then decay to fill the generated core hole, which leads to various features in this decay process: (i) If the excited state decays back to the same ground state by releasing the same amount of energy as the incident X-ray, it will generate an elastic (no change on energy) feature (Fig. 1a left). (ii) If the decay corresponds to filling up the core hole by a valence-band electron, the emitted photon energy will be pinned by the energy difference between the valence electron and the core hole, independent of the incident X-ray. This is called normal X-ray emission

spectroscopy (XES) or normal fluorescence (Fig. 1a middle). Experimentally, XES is typically collected by exciting the core electron to the high-energy continuum well above the absorption threshold. (iii) In order to maintain the excited state after the absorption process, the core hole of the intermediate state exerts a strong potential to the outer shell electrons to screen itself. Such an effect could lead to various other excitations at much lower energy scale, such as lattice vibrations (phonons), spin flips (spinons or magnons), and charge transfer excitations. When the core hole is eventually filled, these excitations are left in the system, leading to an energy loss of the emitted photon energy compared with the incident X-ray. Therefore, through the excitation (absorption) and decay process, the system may reach three different types of final states (Fig. 1b).

2.2 sXAS and XES detect the unoccupied and occupied states

Various information of the outer-shell electron states of a material could be obtained by detecting the emitted photons. The total count of the emitted photons is actually the fluorescence yield signal in sXAS experiments, which naively corresponds to the unoccupied conduction-band states with the core-hole existence. XES, on the other hand, corresponds to the occupied valence-band states because it mainly involves the decay from valence-band electrons to the core hole. Therefore, the combination of sXAS and XES probe both the unoccupied and occupied states in the vicinity of the Fermi level [25].

The applications of sXAS and XES for studying battery interfaces and materials have been reviewed in more details with examples before [22-24]. Here, we only point out that the occupied/unoccupied states close to Fermi level in the discharged/charged states in electrodes are the most relevant electron states to batteries, because electrons are removed/added from/to these states during the electrochemical operations. Often the

concern of the safety in Li-ion batteries is on the oxygen stability because oxygen occupied state may stay too close to Fermi level and get oxidized during the deintercalation process [26]. As an example, the XES of $LiFePO_4$ displays an interesting reshuffling of the Fe-*3d* occupied states due to specific spin configurations and el-el Coulomb interactions, resulting in an occupied Fe-*3d* state close to the Fermi level. This guarantees that the key electron states involved in the electrochemical charging are dominated by Fe-*3d* states in $LiFePO_4$, which naturally provides the fundamental rationality on "Why $LiFePO_4$ is a safe battery electrode" [27].

2.3 Technical comparison between mRIXS and sXAS

As explained in Fig. 1, RIXS results contain the information of three types of decay processes and their associated excitations. In fact, RIXS has been used as a powerful technique for probing low-energy excitations in fundamental physics [28-30]. Because RIXS does not directly represent a static configuration of electron density of states, understanding RIXS often requires complicated theoretical approaches. However, through a direct comparison of RIXS results with conventional sXAS data (Fig. 2), one could easily understand the technical meaning of RIXS, and why it is an elemental and orbital sensitive tool with superior chemical sensitivity than conventional sXAS.

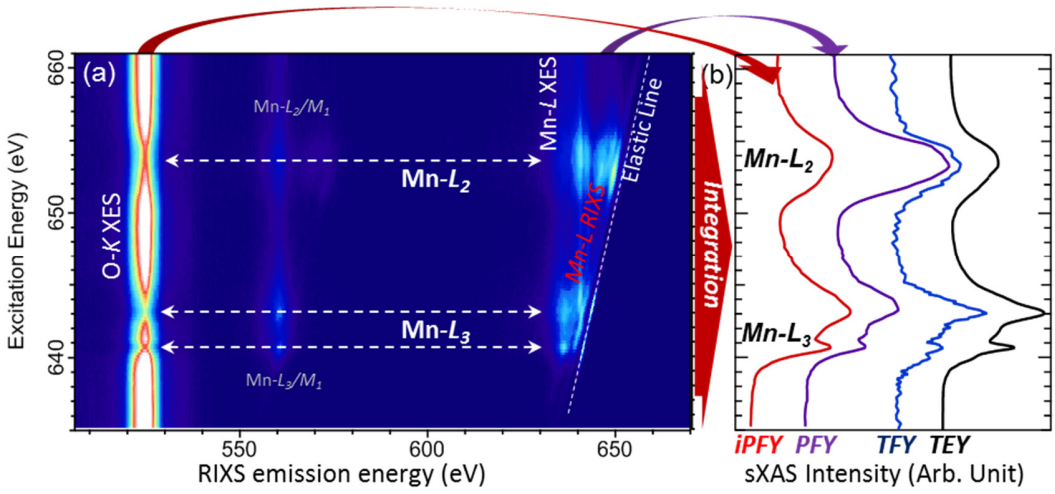

Fig. 2 (a) mRIXS collected from $LiNi_{1/3}Mn_{1/3}Co_{1/3}O_2$ with incident X-ray excitation energy at the Mn-*L* edge range (vertical axis). Horizontal axis is the energy of the emitted photons detected by a RIXS spectrometer. Color indicates the intensity distribution of the emitted photons, with light color represents high intensity [31]. **(b)** Integration of mRIXS intensity along horizontal direction leads to different types of sXAS spectra. The conventional sXAS from total electron yield (TEY) and total fluorescence yield (TFY) channels are plotted for comparison. TFY spectrum is severely distorted due to the competing contributions from both O and Mn (white arrows in (a)). Depending on which section the mRIXS intensity is integrated, partial fluorescence yield (PFY) and inverse partial fluorescence yield (iPFY) could be obtained by integrating the intensity in the Mn-*L* and O-*K* emission range, respectively. Note iPFY is a bulk-probe PIPO channel without any lineshape distortion found in TFY sXAS.

Fig. 2 presents a direct comparison between mRIXS and various sXAS spectra of a $LiNi_{1/3}Mn_{1/3}Co_{1/3}O_2$ electrodes with incident X-ray energy (vertical axis) at the Mn-*L* range. At each incident energy, the emitted photons from the sample are differentiated by a RIXS spectrometer upon their emission energies (horizontal axis). Therefore, if one integrates all the RIXS intensity with the same excitation energy (horizontal integration), it will generate

a single spectrum of Mn-*L* sXAS. Depending on the range of emission energy for such an integration, different channels of sXAS signals could be obtained simultaneously: Integration in the Mn-*L* emission energy range from 630 to 650 eV generates the partial fluorescence yield (PFY) sXAS. The inverse of the integrated intensity in the O-*K* range, 520-530 eV, generates the inverse partial fluorescence yield (iPFY) sXAS. The integration of all the RIXS intensity is the total fluorescence yield (TFY) of sXAS.

Several important messages emerge through the comparison in Fig. 2. First, with the same excitation energy, RIXS further resolves the single data point in sXAS into an energy distribution curve. RIXS therefore provides a new dimension of information along emission energy that is completely missing in sXAS. As shown throughout this review, this provides extra sensitivity to the chemical states in battery materials. Second, it is clear that the "elemental sensitive" of the sXAS does not necessarily mean all signals are from the same element in the material. Here, Mn-*L* sXAS contains significant contribution of emissions from oxygen. Such a mixing of emission signals in sXAS is the direct reason of the severe distortion of the TFY sXAS spectral lineshape, because the intensity change of the O and Mn contributions are exactly opposite (white arrows in Fig. 2a) due to the sudden change of the attenuation length at an absorption edge. Third, it is worth noting that, as shown by the seminal work of Achkar et al. with silicon-drift detector, iPFY is a bulk probe of sXAS without any lineshape distortion [32]. This makes iPFY particularly useful for quantitative analysis of the bulk TM states, and mRIXS enables iPFY of all edges through its much improved emission energy resolution. Fourth, resolving the emission energy in mRIXS enables a new dimension for differentiating critical RIXS features within a particular emission energy range, allowing a more detailed study of a particular chemical

state that could be completely buried in sXAS. If such an emission energy range is very small, e.g., in one or two eVs, the generated spectrum, dubbed super-partial fluorescence yield (sPFY), becomes intrinsically different from the conventional sXAS. While sPFY is actually RIXS signals plotted upon the same sXAS axis, it provides unique technical capabilities to quantify specific RIXS features for chemistry and material studies. Fifth, other unpopular decay channels could also be detected in such high-efficiency mRIXS. For example, decays from Mn 3s to 2p states (dipole allowed) are shown in the mRIXS around 560 eV emission energy (Fig. 2a). Such a core-core partial fluorescence yield (ccPFY) provides another channel for obtaining non-distorted sXAS bulk signal [33], especially when iPFY cannot be implemented due to the lack or low-energy edges.

RIXS is a photon-hungry technique, due to the low branching ratio of the particular core hole decay channel involved. This is the reason why XES, discovered in 1934 since the early days of quantum mechanics[34], was largely replaced by x-ray photoelectron spectroscopy (XPS) until the third generation synchrotron light source was developed. RIXS has made remarkable progress and provided invaluable contributions to the fields of highly correlated physics in the last two decades [28-30]. Today's mRIXS was made possible through the recent developments of ultra-high efficiency spectrographs in the soft X-ray range [31, 35, 36]. Other than the superior chemical sensitivity of mRIXS, the many new sXAS channels beyond conventional TEY, TFY and PFY signals, e.g., iPFY, sPFY, ccPFY as explained above, are simply byproducts of mRIXS, and they open up new opportunities for studying both the surface and bulk chemistry of energy materials through soft X-rays, as demonstrated by the examples below.

3. SXS for Surfaces and Interfaces

3.1 Surfaces and interfaces probed by sXAS

Interfaces play critical roles in all the battery operation. Decades of fundamental studies and practical tests have been performed to understand and optimize the battery interfaces in both academia and industry. In conventional batteries with liquid electrolyte, the so-called solid-electrolyte interphase (SEI) on the anode surface is formed through electrolyte decomposition during the early cycles. The SEI behaves as a passivation layer to stabilize the battery operation by preventing electron transportation but allowing efficient ion diffusion and depletion [37]. For the cathode, especially high voltage compounds, the surface reconstruction and surface layer formation have also attracted much research attention. Surface treatments and modifications have been implemented for most commercial cathodes, but the control and optimization of the electrode surface for a stable high-voltage operation remain a major technical challenge [38]. For SSBs, understanding and optimizing the electrode-electrolyte interface (EEI) becomes critical due to the inherent challenge from a relatively poor solid-solid mechanical contact [7-9].

Due to the shallow escape depth of electrons, the total electron yield (TEY) channel of sXAS is a surface sensitive probe with probe depth of about 10 nm. The contrast between TEY and TFY (probe depth of about 100 nm) often provides valuable information on the surface and interface chemistry in batteries [23, 24]. Such experiments are based on the sensitivity of sXAS to the relevant chemical species and chemical bonds. For example, sXAS directly reveals the distinct chemical composition of the SEIs formed on Sn anodes with different surface orientation, with carbonates and fluorides on the Sn (100) and (001) surfaces from different decomposition reactions of the solvent and salt, respectively [39].

sXAS analysis also shows that the formation process of SEI could be much more complex than a continuous deposition of the electrolyte decomposition products. The SEI could evolve upon electrochemical potentials during the formation process and displays an oscillating growth pattern in both the chemical compositions and thickness [40]. Benefiting from the shallow probe depth, sXAS also allows the investigation of the chemical contrast of the different electrode surfaces facing electrolyte and current collector at high voltages [41], and specific molecular configurations on electrode surfaces [42].

sXAS in TEY and TFY channels have also been used to study the surface behavior of solid electrolyte particles used for SSBs [43, 44]. For example, an counterintuitive air-exposure effect was found on Al-substituted $Li_7La_3Zr_2O_{12}$ (LLZO) particle surface through the sXAS studies by Cheng et al. [43]. By evaluating the contribution ratio of the O-*K* features from the LLZO and carbonates, sXAS suggests that much less carbonates are formed on the small-grain sample than on the large-grain samples. This is interesting because small-size particles with large specific surface area are typically more prone to the surface reaction upon air exposure than large particles. Further experimental and theoretical analysis reveals that the surface of the small LLZO particles contains less lithium and more aluminum than that of the large particles, leading to a less air-sensitive surface. Additionally, considering the 10 nm probe depth of the TEY channel of sXAS, the thickness of the carbonate coating could be roughly estimated to be couple nm for the LLZO solid electrolyte particles [44].

3.2 RIXS for detecting subtle chemical changes

While sXAS remains a sensitive tool for detecting the surface chemistry of many systems, we would like to emphasize that, often the chemistry at the interface of two

chemical species only shows subtle but critical difference compared with the bulk materials involved. It could be technically challenging to detect such weak contrast through conventional sXAS. One of the extreme case is to detect the ion-solvation shell in liquid electrolyte, where the molecules in the solvation shell (the "interface" of ions and liquid) are essentially the same as in the bulk electrolyte. The ion-solvation shell is a critical configuration in conventional battery systems, and is directly involved in the charge transfer process throughout the electrochemical operations [37, 45]. Unfortunately, experimental detection of the solvation shell remains one of the grand challenges. Fig. 3 displays the sXAS and RIXS spectra of a model aqueous system with different KCl salt concentrations [46]. As expected, the sXAS spectral lineshape does not change much for different salt concentrations, and shows characteristic pre- (~534 eV), main- (~536 eV), and post-edge (~540 eV) features that are typical for water. This is expected because the O-*K* sXAS measured here are from the solvent molecule, water, which is the same for pure water and the water in the ion solvation shells. In contrast, a significant change could be observed in the RIXS spectra collected at the 534.2 eV excitation energy (one horizontal cut in mRIXS as explained in Fig. 2). The strong evolution of the RIXS spectral weight towards 534.2 eV emission energy (elastic peak) suggests that low-energy excitations of vibrational modes (phonons) in RIXS are greatly suppressed in the ion-solvation shell, and higher resolution analysis of the phonon excitations in RIXS could shed light on the details of the molecular configuration in the solvation shell [46]. Such strong spectral changes, however, are completely missing in the sXAS data because, technically, the integrated area of the RIXS spectra are roughly the same after normalization. This example is thus a typical

demonstration of the superior chemical sensitivity of RIXS for interface studies due to the new dimension of emission energy distributions in RIXS.

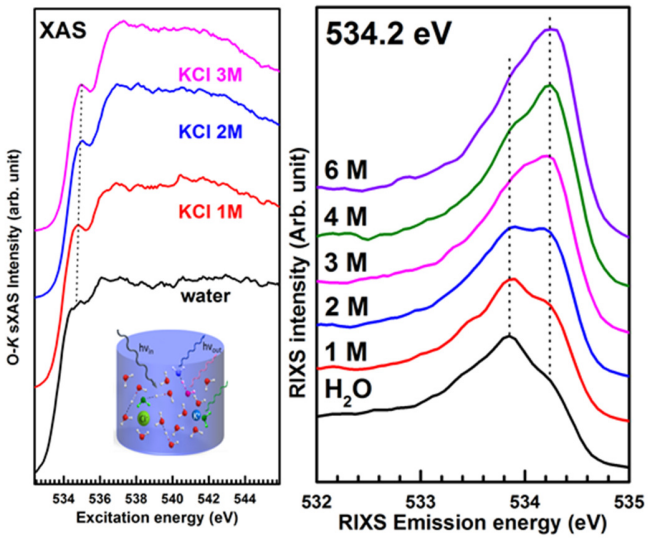

Fig. 3 *In situ* sXAS and RIXS of a model aqueous salt solution with different KCl salt concentrations. **(a)** The sXAS displays more or less the same lineshape with different salt concentrations. **(b)** The RIXS cuts at 534.2 eV excitation energy (dotted line in sXAS) show a dramatic lineshape change along the emission energy due to the ion-solvation effect [46].

4. SXS for Probing Cationic Redox

4.1 Quantitative analysis of TM redox through sXAS

Compared with hard X-ray XAS, one of the inherent advantages of TM *L*-edge SXS is the strong dipole-allowed TM *2p-3d* excitations, leading to arguably the most direct probe of the oxidation state of *3d* TMs in battery compounds [22]. The TM *L*-edge spectral lineshapes are defined largely by atomic multiplet effects [47] and therefore sharp and well-defined features can be observed via sXAS. The high sensitivity and well-defined features of TM sXAS enable various kinds of *in-situ/operando* and microscopic studies of the TM oxidation states [48-50]. Additionally, lineshape analysis of the sharp multiplet features in

TM-*L* sXAS provides so far the most reliable quantification of the *3d* TM oxidation state distributions in battery materials at different electrochemical stages [51].

Fig. 4 is a summary of three selected examples of quantitative soft sXAS studies of Mn, Fe, and Ni cations in battery cathodes. A perfect quantitative fitting of all the high-resolution sXAS experimental features could be achieved through a simple linear combination of multiple reference spectra (for Mn, Fig. 4a) [41, 52, 53], two end-members for two-phase systems (for Fe, Fig. 4b) [54], or theoretical calculations of the TFY spectra (For Ni TFY, Fig. 4c) [55]. Even for the more complicated Co system that is of more solid-solution type, quasi-quantitative analysis could be achieved by the main peak position [51, 56, 57]. Such quantitative analysis could reveal some key TM species on the surface of the electrodes [58], and define unambiguously the TM redox involved in electrode cycling, as specifically reviewed before for most *3d* TMs in battery materials [51].

However, although powerful as a surface sensitive probe, technical challenges remain for a reliable detection of the bulk TM redox, due to the inherent lineshape distortion in the bulk-sensitive sXAS TFY channel. As directly shown in Fig. 2, the distortion is particular severe for TMs with other edges close by, e.g., Mn [32], and developments of iPFY and ccPFY become critical for a non-distorted bulk sXAS detection channel [32, 33, 59]. We note again that, with the high resolution of the emission energy, mRIXS naturally includes both iPFY and ccPFY signals of all TM-*L* sXAS. The quantitative sXAS analysis demonstrated here could thus be extended to bulk TM analysis in exactly the same way but based on iPFY and/or ccPFY experimental data from mRIXS.

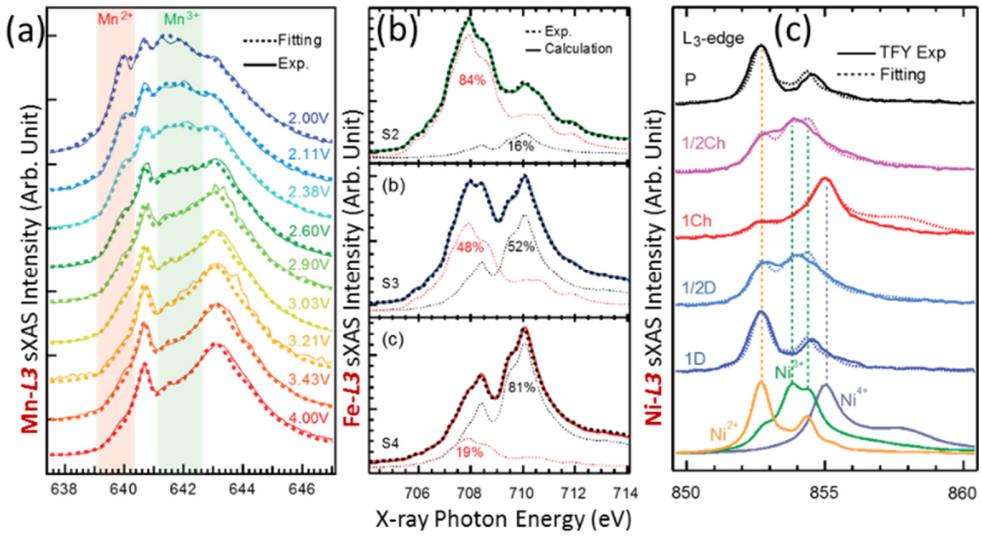

Fig. 4 (a) Quantitative definition of TM oxidation states of (a) Mn, (b) Fe, and (c) Ni in battery electrodes at different electrochemical stages. All fittings are based on simple linear combinations of reference spectra from either experiments or theory. All fittings show perfect agreement with experimental sXAS data, indicating a precise and reliable quantification of TM states in battery materials [22, 54, 58, 60]. It is important to note that such a simple approach could be extended to the quantitative analysis of iPFY and ccPFY directly for studying TMs in bulk materials.

4.2 mRIXS of unusual TM redox

Compared with sXAS, the new information by introducing the emission energy into mRIXS naturally provides another dimension to resolve the entangled states in sXAS. This becomes particularly important for determining the novel redox couples of both TMs and oxygen. Such an advantage of mRIXS is directly shown in Fig. 5, where a 90-year speculation of Mn^{1+} state in coordinated compound is clearly revealed in a charged battery electrode through mRIXS, but not sXAS [61].

The sXAS and mRIXS collected on a charged and discharged anode with a Prussian Blue Analogue material, $Na_{1.24}Mn[Mn(CN)_6]\bullet 2.1H_2O$, are shown in Fig. 5. An intriguing

low-voltage plateau is found through the Na-ion intercalation with an excellent rate performance, which suggests that this material could be used as a high-rate Na-ion battery anode with very low production cost [61]. Further reduction of the pristine Mn^{2+} to Mn^{1+} through the ion intercalation is very unusual because Mn typically takes only zero or bivalence states. In fact, Mn^{1+} was proposed in such coordinated compounds since 1928 [62], but was not verified experimentally through conventional spectroscopy including XPS and sXAS. Because the spin states of the TMs in such material could be well defined depending on their coordination sites, such material displays distinct signatures of the typical TM states in sXAS [63-65]. However, for such novel chemical state, the contrast on the sXAS is very weak for the cycled electrodes (Fig. 5). Only a hint of difference around 643.5 eV could be seen, although the lineshape change does correspond to the $Mn^{2+/1+}$ states expected by multiplet theory [61]. In sharp contrast, the mRIXS reveals distinct features of the charged electrode that corresponds to the *d-d* excitations (excitation of an occupied TM *3d* electron to an unoccupied state within the *3d* orbitals) of a low-spin Mn^{1+} system, thus providing the ultimate experimental verification of the $Mn^{1+/2+}$ redox in the anode [61]. This demonstration not only showcase the power of mRIXS for revealing novel chemistry, more importantly, it directly confirms that chemical states in battery environment could be well beyond what we would expect in conventional systems.

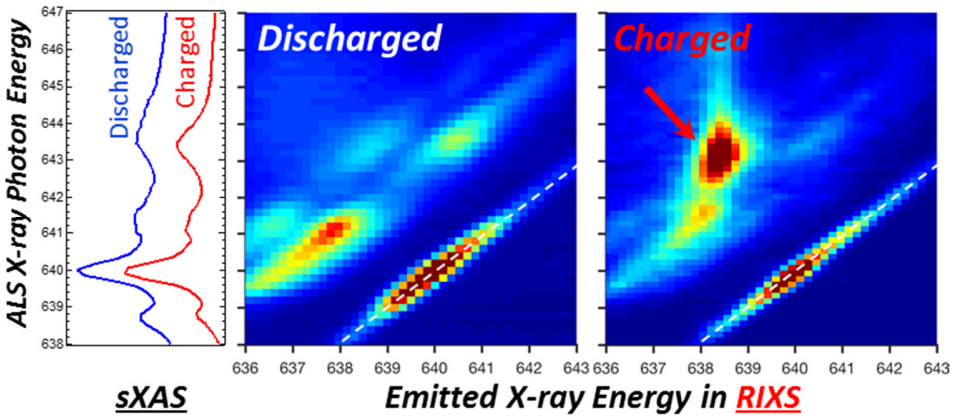

Fig. 5 The SXS contrast between a discharged and charged anode based on a Prussian Blue Analogue material, $Na_{1.24}Mn[Mn(CN)_6]$. A small contrast in sXAS could be seen around 643.5 eV photon energy (vertical axis), but mRIXS shows a significant intensity redistribution, indicating a novel $Mn^{1+/2+}$ redox in this anode material [61].

5. mRIXS fingerprints Anionic Redox

Anionic redox, i.e., oxygen redox in oxide cathodes, holds a promise of delivering much higher capacity and power compared with the conventional TM redox based batteries [11], provided the oxygen redox could be maintained to be stable and reversible. In general, the evolution of oxygen has long been a critical topic in battery field ever since the first-generation Li-ion battery with $LiCoO_2$ cathode, however, has typically been considered detrimental to the stability of battery materials. Reversibility is the most critical parameter on whether the intensive effort on studying oxygen redox in batteries is meaningful at all. A crucial question associated with this concern is whether the oxygen redox mechanism naturally triggers the unfavorable oxygen evolution and gas release in batteries. Therefore, detecting and understanding the fundamental mechanism of the oxygen redox involved in battery electrodes have recently become one of the most pursued topics in the battery field.

At this time, several controversy models based on structural change and chemical configurations have been proposed [12-21].

5.1 Why O-K sXAS is not a reliable probe of oxygen redox?

Due to the inherent elemental sensitivity, O-*K* spectroscopy including XPS and sXAS have quickly become popular tools to tackle oxygen redox issues in many high-profile publications. Here, we first clarify the inherent problems with such conventional spectroscopy and we believe the controversy on understanding oxygen redox is partially due to the fact that these techniques, although popular in the battery field, are not reliable probes for studying bulk oxygen redox.

Discussions on oxygen redox based on O-*K* sXAS have focused on either the intensity or the lineshape of the so-called "pre-edge" features below 535 eV. Firstly, the seminal 1989 work by Frank de Groot et al. concluded that these features are "related to the metal 3d states" [66]. Decades of spectroscopic studies have confirmed that these features are from TM-*3d* states hybridized to O-*2p* states, which is then involved in the O-*K* sXAS. The intensity (area) of the pre-edge features is dominated by the strength of the hybridization, which is naturally enhanced in charged states because the high valence state of the TMs results in stronger hybridizations with O. This is most clearly shown by the contrast of charged and discharged $LiFePO_4$, where obvious pre-edge features including two peaks is shown in O-*K* sXAS of charged electrodes, in sharp contrast with the negligible pre-edge intensity of the discharged state (Fig. 6a) [27, 67]. Such a pre-edge area enhancement due to strengthened hybridization during the charging process has been found almost universally for electrodes with or without oxygen redox, e.g., olivine, spinel, and non-Li-rich layered compounds [27, 55, 67-70]. Quantitatively, the area analysis of these features

shows that the intensity increases even before the oxygen redox voltage is reached [17, 18], also indicating it is merely from the enhanced hybridization from the increasing TM valence, not a signature of oxygen redox.

Secondly, the lineshape change of the O-*K* pre-edge features upon cycling are due to two factors. One is the overall broadening of the spectral features due to the enhanced hybridization and covalency in charged states as described above. The other is that the changed TM valence upon cycling also changes the O-*K* pre-edge peak positions, leading to different lineshapes. A typical example of such lineshape changes could be seen in Fig. 6b collected on spinel $LiNi_{0.5}Mn_{1.5}O_4$ electrodes. Besides the overall intensity enhancement, an extra feature emerges at a low energy in charged state due to the highly oxidized Ni^{4+} (Fig. 6b) [55, 70, 71]. Therefore, the overall broadening and lineshape changes are also predominantly from TM changes, not signatures of oxygen redox.

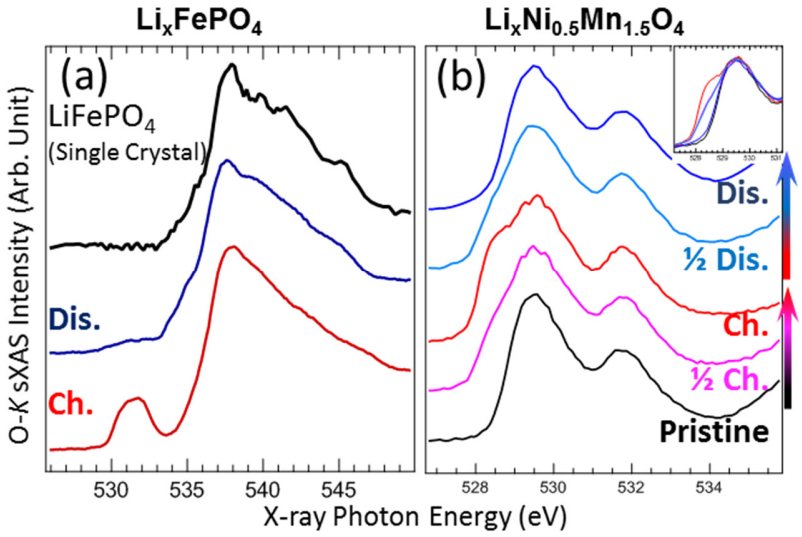

Fig. 6 O-K sXAS spectra collected from charged (Ch.) and discharged (Dis.) electrodes of (a) olivine LiFePO4 [27], and (b) spinel $Li_xNi_{0.5}Mn_{1.5}O_4$ [55]. Strong variation in the area intensity and lineshape could be observed for the pre-edge features below 535 eV without involving oxygen

redox. In fact, such changes are almost universal in battery electrodes, stemming from the increasing TM valence and thus the TM-O hybridization upon charge.

While we show that neither the intensity nor the lineshape of the O-K pre-edge features is a reliable probe of oxygen redox, there is an important point to clarify. The sXAS feature of oxidized oxygen in reference compounds, e.g., Li_2O_2 and O_2, was indeed found to be around 531 eV within the same energy range as the pre-edge features [72-74]. In fact, arguments based on possible Li_2O_2 feature contribution have been used for some meaningful discussions on oxygen redox [75-77]. Unfortunately, the possible peroxide contribution cannot be conclusive due to the dominating effects on both the peak broadness and position changes, as explained above, and it cannot differentiate the specific oxidized oxygen state either [72-74]. In another word, the oxygen redox feature is indeed concealed in the O-*K* pre-edge regime, but unfortunately cannot be distinguished through sXAS due to the dominating effects from TM states in both the intensity and lineshape. The critical challenge is thus to differentiate the intrinsic oxygen redox feature from the strong hybridization features.

5.2 mRIXS to fingerprint the oxygen redox

As elaborated by Fig. 2, mRIXS is a technique that further deciphers the single data spot of a particle counting number in sXAS into a full spectrum upon a new dimension of the emission energy. This provides the superior chemical sensitivity to distinguish specific chemical states that cannot be clearly defined in sXAS (Fig. 3 and 5). Such an improvement is exactly what we need to tackle the entangled oxygen redox and TM-O hybridization features in sXAS pre-edge regime. Additionally, mRIXS is a PIPO technique with probe depth of about 100 nm in the O-*K* range. Compared with PIPO sXAS, the bulk sensitivity

of mRIXS could be further enhanced if the bulk signal is differentiated from surface signal on the emission energy, which is fortunately the case for oxygen redox features, as discussed in this section. Therefore, mRIXS is technically an ideal tool to reveal the true nature of the oxygen redox in battery electrodes.

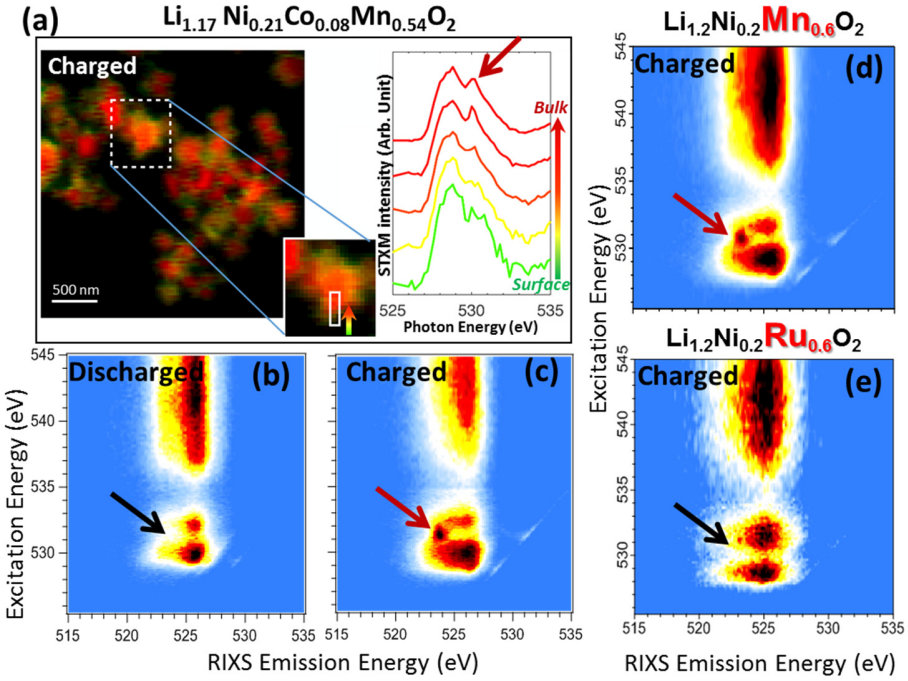

Fig. 7 (a) spatially resolved STXM spectra measured from the surface to the bulk of a charged $Li_{1.17}Ni_{0.21}Co_{0.08}Mn_{0.54}O_2$ particle. A 531 eV peak shows up in the bulk signal (red arrow). (b) and (c) show the contrast in mRIXS of the discharged and charged electrodes on a sharp feature at 531 eV excitation and 523.8 eV emission energy, corresponding directly to the bulk oxygen feature [78]. (d) and (e) show the mRIXS of charged $Li_{1.2}Ni_{0.2}Mn_{0.6}O_2$ and $Li_{1.2}Ni_{0.2}Mn_{0.6}O_2$ electrodes, one with and one without the specific oxygen redox feature, respectively [79]. Arrows indicate the disappearance (black) and appearance (red) of the oxygen redox mRIXS feature.

In Fig. 7a-c, we compare the spatially resolved scanning transmission X-ray microscopy (STXM) with mRIXS of $Li_{1.17}Ni_{0.21}Co_{0.08}Mn_{0.54}O_2$ [78]. STXM shows that a

531 eV feature emerges when the probe switches from the surface of a charged particle to the bulk area (Fig. 7a). However, such feature is completely buried in the conventional sXAS data in either TFY and TEY mode. More strikingly, mRIXS shows a sharp feature with the corresponding excitation energy, only when the electrode is charged to the high voltage (Fig. 7c), below which, no such feature could be observed (Fig. 7b). Systematic mRIXS experiments at different electrochemical stages confirm that this particular feature fingerprints precisely the oxygen redox behavior in electrochemical cycling upon voltages and in charge/discharge states for extended cycles [78]. The comparison with STXM is a direct proof that, although RIXS has nominally the same probe depth as TFY sXAS, the specific oxygen redox feature observed in mRIXS corresponds to only the bulk oxygen signal. The fact that no corresponding signal from this mRIXS feature could be seen in the STXM collected on the particle surface also shows that surface behavior, e.g., contributions in XPS, of the battery electrode is irrelevant to the bulk oxygen redox.

The mRIXS observations are consistent with the single-energy cut of RIXS at 531 eV excitation energy [17, 18]. However, mRIXS provides the full profile of the oxygen redox feature along both excitation and emission energy, which is critical for its theoretical interpretation to reveal the fundamental mechanism of the oxygen redox. Compared with STXM, RIXS experiments could be performed directly on any battery electrodes at different electrochemical stages, instead of the TEM-style samples for STXM. At this time, among all O-*K* core level spectroscopy techniques, mRIXS provides the only direct elemental and bulk sensitive probe of the oxygen redox that could be employed to all battery electrodes.

There are several crucial mRIXS observations on the oxygen redox feature:

1. Regardless of the types of TMs (*3d* or *4d*) that are involved in the oxide electrodes, e.g., $Li_{1.2}Ni_{0.2}Mn_{0.6}O_2$ and Li_2RuO_3, once the oxygen redox is activated in the electrode, the different systems display the same mRIXS feature. This strongly indicates a universal mechanism that fundamentally drives the oxygen redox in all the electrode systems. Theoretical simulation that could directly reproduce the mRIXS feature is the key to reveal this fundamental mechanism.

2. On the other hand, the activation of oxygen redox strongly depends on the TM compositions. However, this TM dependence does not simply reflect a TM-O hybridization model. For example, changing Mn to Ru in $Li_{1.2}Ni_{0.2}M_{0.6}O_2$ (M=Mn, Ru) completely suppresses the oxygen redox as revealed by mRIXS (Fig. 7d,e). mRIXS confirms that $Li_{1.2}Ni_{0.2}Mn_{0.6}O_2$ is oxygen redox active; however, Ru is the active cationic redox in the $Li_{1.2}Ni_{0.2}Ru_{0.6}O_2$ without oxygen redox [79].

3. The intrinsic oxygen redox feature in mRIXS is a sharp feature at 523.8 eV emission energy, which is clearly separated from the broad TM-O hybridization features typically found at 525 eV for oxide RIXS, as extensively reported in fundamental physics field [80]. The highly localized nature of the RIXS feature, in both incident (excitation) and scattered (emission) photon energies, indicates that hybridization effects may only be tangentially related to the feature, as corroborating by the relative insensitivity of the feature across *3d* and *4d* TM elements.

4. Conventional wisdom often associates the oxygen redox with the high-voltage plateau, especially in Li-rich compounds. However, mRIXS results over extended cycles clearly reveal that oxygen redox remains in the system even

without the high-voltage plateau [78]. The dissociation of the oxygen redox from the high-voltage plateau is a critical finding for opening up new opportunities for further material explorations and optimization.

5. The independence of TMs on the oxygen-redox feature (#1) and the dependence of TMs on the activation of oxygen redox (#2) imply that the mechanism is more complex than what has been proposed so far. At this time, the universal and fundamental mechanism is yet to be revealed, so the effects from structure, TM compositions, and local chemical configurations are individually discussed in different proposals, leading to the controversy. A fundamental foundation of a strategically architectural mechanism is the key to take the mystery out of the oxygen redox, and to explore the possibilities on its practical potential.

Although the theoretical interpretation of the mRIXS feature remains a nontrivial issue, and as mentioned before, even the sPFY/STXM 531 eV signal originates from a RIXS feature that is intrinsically different from sXAS, the precise correlation between the mRIXS feature and the electrochemical cycling strongly suggests that mRIXS is the tool-of-choice for detecting the bulk anionic redox in battery electrodes. While mRIXS observations imply a complex mechanism than just a single model, the optimism lies in the clear and reliable observation through mRIXS. A direct simulation of the mRIXS oxygen-redox feature holds the promise to reveal the true fundamental nature of oxygen redox, which will lead to the ultimate understanding of oxygen redox by further incorporating other factors like structure and specific chemical configurations.

6. Opportunities and Perspectives on SXS of SSB

While most examples shown in this review are not directly on SSB systems, all these demonstrations could be extended to SSB systems directly. In addition, because of the inherent requirement of ultra-high vacuum for most soft X-ray detection channels, solid electrolyte is naturally a blessing for *in-situ/operando* SXS experiments on real-world SSBs. Today's SXS techniques have greatly advanced, and experiments of liquid and gaseous phases could be measured with sophisticated *in-situ* cells, as extensively reported and reviewed previously [81-86]. However, due to the shallow penetration length of soft X-rays, cells built on very thin (typically 100 nm thickness) membrane window is typically required for liquid/gas experiments. With solid-state electrolyte, such a complication could be avoided and SXS experiments could be performed directly on a real-world battery by designing the top layer in the schematic of Fig. 8. For example, controlled micrometer sized detection windows could be fabricated on a typical metal foil current collector for measuring the electrode materials. In order to avoid the relaxation effect inside the open windows for some materials [50], A thin film top-layer of metal, e.g., Al, or Au, could also serve as the current collector while allowing most soft X-ray photons passing through. In particular, if the electrode deposition is also controlled to achieve an electrode thickness of less than 100 nm, *in-situ/operando* PIPO SXS could reach the electrode-electrolyte interface directly. With the superior chemical sensitivity of mRIXS, we expect unprecedented information will be uncovered on both the bulk electrodes and interfaces in SSB systems.

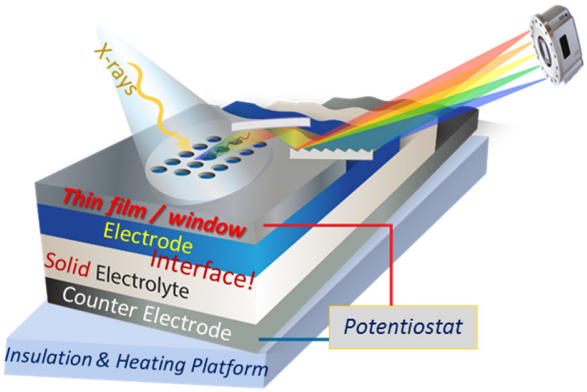

Fig. 8 Schematic of a typical *in-situ/operando* SXS experiment based on SSB cells. Top layer could either be conventional current collector with detection windows, mesh current collector, or a thin film of Al or Au. Controlled thickness of the electrode will allow the probe depth to reach the electrode-electrolyte interface.

7. Conclusions

This review provides a comprehensive summary in both the techniques and analysis of the state-of-art SXS for revealing the critical chemistry in batteries. Through a direct comparison with sXAS, mRIXS is introduced for battery researches and is explicated as further resolved sXAS signals along a new energy dimension, the emission energy. In addition to the conventional TEY and TFY channels of sXAS, mRIXS simultaneously contains four more types of PIPO signals, i.e., PFY, iPFY, sPFY and ccPFY. The combination of these signal channels provides complete and powerful characterizations of both the surface/interface and the bulk properties of battery materials.

We discuss several recent demonstrations in three aspects. On the surface and interfaces, we show that sXAS is sensitive to particular chemical bonds on the material surface, and RIXS could distinguish even the subtle chemical contrast between the ion-solvation shell and bulk electrolyte. On the cationic redox reactions, we show that quantitative definitions

of the TM states at different electrochemical states could be achieved through a simple linear-combination fitting, which is made possible by the high sensitivity of the sharp features in TM-*L* sXAS to the TM oxidation states. However, some novel TM states, e.g., Mn^{1+}, cannot be clearly identified by sXAS, but could be revealed by mRIXS along the new dimension of emission energy. On the anionic oxygen redox reactions, we first clarify explicitly that neither the intensity nor the lineshape of the O-*K* sXAS pre-edge features should be used as evidence of oxygen redox, which is currently a popular approach found in many high-profile publications. The only reliable spectroscopic probe of oxygen redox we found so far is a specific feature in mRIXS. We discuss some important observations through mRIXS on understanding the oxygen redox, and provide our perspectives. The interpretation of the mRIXS feature is the key to uncover the fundamental and universal nature of oxygen redox in various electrode systems, only after which, the ultimate understanding of the oxygen redox could be achieved by further considerations of other factors like the structure and chemical configurations. Nonetheless, mRIXS is the tool-of-choice for tackling both the material's oxygen activities and points to a clear direction on the fundamental understanding of oxygen redox.

Because SSB systems allow *in-situ/operando* SXS experiments performed without the typical membrane windows, they provide unique opportunities for studying real-world electrode materials and the interfaces in SSBs. We foresee that applications of advanced SXS techniques reviewed in this work will lead to significant contributions to chemical characterizations, fundamental understandings and material explorations for a broad range of topics in advanced battery technologies.

ACKNOWLEDGMENTS

This research used resources of the Advanced Light Source, which is a DOE Office of Science User Facility under contract no. DE-AC02-05CH11231. We acknowledge support from the U.S. Department of Energy, Office of Basic Energy Sciences, Division of Materials Sciences and Engineering under Contract No. DE-AC02-76SF00515.

[1] H. Li, J. Janek, A. Manthiram, Solid State Ion., DOI: 10.1016/j.ssi.2017.12.025 (2018) In press.
[2] A. Manthiram, X. Yu, S. Wang, Nat. Rev. Mater., 2 (2017) 16103.
[3] J. Janek, W.G. Zeier, Nat. Energy, 1 (2016) 16141.
[4] L. Fan, S. Wei, S. Li, Q. Li, Y. Lu, Adv. Energy Mater., 2018 (2018) 1702657.
[5] A. Mauger, M. Armand, C.M. Julien, K. Zaghib, J. Power Sources, 353 (2017) 333-342.
[6] J.G. Kim, B. Son, S. Mukherjee, N. Schuppert, A. Bates, O. Kwon, M.J. Choi, H.Y. Chung, S. Park, J. Power Sources, 282 (2015) 299-322.
[7] J.C. Bachman, S. Muy, A. Grimaud, H.H. Chang, N. Pour, S.F. Lux, O. Paschos, F. Maglia, S. Lupart, P. Lamp, L. Giordano, Y. Shao-Horn, Chem. Rev., 116 (2016) 140-162.
[8] C. Sun, J. Liu, Y. Gong, D.P. Wilkinson, J. Zhang, Nano Energy, 33 (2017) 363-386.
[9] E. Quartarone, P. Mustarelli, Chem. Soc. Rev., 40 (2011) 2525-2540.
[10] C. Ma, Y. Cheng, K. Chen, J. Li, B.G. Sumpter, C.-W. Nan, K.L. More, N.J. Dudney, M. Chi, Adv. Energy Mater., 6 (2016) 1600053.
[11] A. Grimaud, W.T. Hong, Y. Shao-Horn, J.M. Tarascon, Nat. Mater., 15 (2016) 121-126.
[12] A.J. Perez, Q. Jacquet, D. Batuk, A. Iadecola, M. Saubanère, G. Rousse, D. Larcher, H. Vezin, M.-L. Doublet, J.-M. Tarascon, Nat. Energy, 2 (2017) 954-962.
[13] P.E. Pearce, A.J. Perez, G. Rousse, M. Saubanere, D. Batuk, D. Foix, E. McCalla, A.M. Abakumov, G. Van Tendeloo, M.L. Doublet, J.M. Tarascon, Nat. Mater., 16 (2017) 580-586.
[14] M. Sathiya, J.B. Leriche, E. Salager, D. Gourier, J.M. Tarascon, H. Vezin, Nat. Commun., 6 (2015) 6276.
[15] E. McCalla, A.M. Abakumov, M. Saubanere, D. Foix, E.J. Berg, G. Rousse, M.L. Doublet, D. Gonbeau, P. Novak, G. Van Tendeloo, R. Dominko, J.M. Tarascon, Science, 350 (2015) 1516-1521.
[16] M. Sathiya, G. Rousse, K. Ramesha, C.P. Laisa, H. Vezin, M.T. Sougrati, M.L. Doublet, D. Foix, D. Gonbeau, W. Walker, A.S. Prakash, M. Ben Hassine, L. Dupont, J.M. Tarascon, Nat. Mater., 12 (2013) 827-835.
[17] K. Luo, M.R. Roberts, R. Hao, N. Guerrini, D.M. Pickup, Y.S. Liu, K. Edstrom, J. Guo, A.V. Chadwick, L.C. Duda, P.G. Bruce, Nat. Chem., 8 (2016) 684-691.
[18] K. Luo, M.R. Roberts, N. Guerrini, N. Tapia-Ruiz, R. Hao, F. Massel, D.M. Pickup, S. Ramos, Y.S. Liu, J. Guo, A.V. Chadwick, L.C. Duda, P.G. Bruce, J. Am. Chem. Soc., 138 (2016) 11211-11218.
[19] J. Lee, J.K. Papp, R.J. Clement, S. Sallis, D.H. Kwon, T. Shi, W. Yang, B.D. McCloskey, G. Ceder, Nat. Commun., 8 (2017) 981.
[20] D.-H. Seo, J. Lee, A. Urban, R. Malik, S. Kang, G. Ceder, Nat. Chem., 8 (2016) 692-697.
[21] M. Okubo, A. Yamada, ACS Appllied Materials & Interfaces, 9 (2017) 36463-36472.

[22] F. Lin, Y. Liu, X. Yu, L. Cheng, A. Singer, O.G. Shpyrko, H.L. Xin, N. Tamura, C. Tian, T.C. Weng, X.Q. Yang, Y.S. Meng, D. Nordlund, W. Yang, M.M. Doeff, Chem. Rev., 117 (2017) 13123-13186.
[23] W. Yang, X. Liu, R. Qiao, P. Olalde-Velasco, J.D. Spear, L. Roseguo, J.X. Pepper, Y.-d. Chuang, J.D. Denlinger, Z. Hussain, J. Electron. Spectrosc. Relat. Phenom., 190 (2013) 64-74.
[24] R. Qiao, W. Yang, J. Electron. Spectrosc. Relat. Phenom., 221 (2017) 58-64.
[25] P. Olalde-Velasco, J. Jimenez-Mier, J.D. Denlinger, Z. Hussain, W.L. Yang, Phys. Rev. B, 83 (2011) 241102.
[26] J.B. Goodenough, Y. Kim, Chem. Mater., 22 (2009) 587-603.
[27] X. Liu, Y.J. Wang, B. Barbiellini, H. Hafiz, S. Basak, J. Liu, T. Richardson, G. Shu, F. Chou, T.C. Weng, D. Nordlund, D. Sokaras, B. Moritz, T.P. Devereaux, R. Qiao, Y.D. Chuang, A. Bansil, Z. Hussain, W. Yang, Phys. Chem. Chem. Phys., 17 (2015) 26369-26377.
[28] A. Kotani, S. Shin, Rev. Mod. Phys., 73 (2001) 203-246.
[29] L.J.P. Ament, M. van Veenendaal, T.P. Devereaux, J.P. Hill, J. van den Brink, Rev. Mod. Phys., 83 (2011) 705.
[30] T.P. Devereaux, R. Hackl, Rev. Mod. Phys., 79 (2007) 175-233.
[31] R. Qiao, Q. Li, Z. Zhuo, S. Sallis, O. Fuchs, M. Blum, LotharWeinhardt, C. Heske, J. Pepper, M. Jones, A. Brown, A. Spucces, K. Chow, B. Smith, P.-A. Glans, Y. Chen, S. Yan, F. Pan, L.F.J. Piper, J. Denlinger, J. Guo, Z. Hussain, Y.-D. Chuang, W. Yang, Rev. Sci. Instrum., 88 (2017) 033106.
[32] A.J. Achkar, T.Z. Regier, H. Wadati, Y.J. Kim, H. Zhang, D.G. Hawthorn, Phys. Rev. B, 83 (2011) 081106.
[33] R. Golnak, J. Xiao, K. Atak, I. Unger, R. Seidel, B. Winter, E.F. Aziz, J. Phys. Chem. A, 120 (2016) 2808-2814.
[34] H.M. O'Bryan, H.W.B. Skinner, Phys. Rev., 45 (1934) 0370-0378.
[35] O. Fuchs, L. Weinhardt, M. Blum, M. Weigand, E. Umbach, M. Bar, C. Heske, J. Denlinger, Y.D. Chuang, W. McKinney, Z. Hussain, E. Gullikson, M. Jones, P. Batson, B. Nelles, R. Follath, Rev. Sci. Instrum., 80 (2009) 063103.
[36] Y.-D. Chuang, Y.-C. Shao, A. Cruz, K. Hanzel, A. Brown, A. Frano, R. Qiao, B. Smith, E. Domning, S.-W. Huang, L.A. Wray, W.-S. Lee, Z.-X. Shen, T.P. Devereaux, J.-W. Chiou, W.-F. Pong, V.V. Yashchuk, E. Gullikson, R. Reininger, W. Yang, J. Guo, R. Duarte, Z. Hussain, Rev. Sci. Instrum., 88 (2017) 013110.
[37] K. Xu, Chem. Rev., 104 (2004) 4303-4418.
[38] J.H. Kim, N.P. Pieczonka, L. Yang, Chemphyschem, 15 (2014) 1940-1954.
[39] R. Qiao, I.T. Lucas, A. Karim, J. Syzdek, X. Liu, W. Chen, K. Persson, R. Kostecki, W. Yang, Adv. Mater. Interf., 1 (2014) 1300115.
[40] Z. Zhuo, P. Lu, C. Delacourt, R. Qiao, K. Xu, F. Pan, S.J. Harris, W. Yang, ChemComm, 54 (2018) 814-817.
[41] R. Qiao, Y. Wang, P. Olalde-Velasco, H. Li, Y.-S. Hu, W. Yang, J. Power Sources, 273 (2015) 1120-1126.
[42] X. Shan, D.S. Charles, Y. Lei, R. Qiao, G. Wang, W. Yang, M. Feygenson, D. Su, X. Teng, Nat. Commun., 7 (2016) 13370.
[43] L. Cheng, C.H. Wu, A. Jarry, W. Chen, Y. Ye, J. Zhu, R. Kostecki, K. Persson, J. Guo, M. Salmeron, G. Chen, M. Doeff, ACS Appl. Mater. Interf., 7 (2015) 17649-17655.
[44] L. Cheng, E.J. Crumlin, W. Chen, R. Qiao, H. Hou, S. Franz Lux, V. Zorba, R. Russo, R. Kostecki, Z. Liu, K. Persson, W. Yang, J. Cabana, T. Richardson, G. Chen, M. Doeff, Phys. Chem. Chem. Phys., 16 (2014) 18294-18300.
[45] K. Xu, Chem. Rev., 114 (2014) 11503-11618.
[46] Y.L. Jeyachandran, F. Meyer, S. Nagarajan, A. Benkert, M. Bär, M. Blum, W. Yang, F. Reinert, C. Heske, L. Weinhardt, M. Zharnikov, J. Phys. Chem. Lett., 5 (2014) 4143-4148.

[47] G. Frank de, Coordin. Chem. Rev., 249 (2005) 31-63.
[48] Y. Li, J.N. Weker, W.E. Gent, D.N. Mueller, J. Lim, D.A. Cogswell, T. Tyliszczak, W.C. Chueh, Adv. Funct. Mater., 25 (2015) 3677-3687.
[49] T.S. Arthur, P.-A. Glans, M. Matsui, R. Zhang, B. Ma, J. Guo, Electrochem. Commun., 24 (2012) 43-46.
[50] X. Liu, D. Wang, G. Liu, V. Srinivasan, Z. Liu, Z. Hussain, W. Yang, Nat. Commun., 4 (2013) 2568.
[51] Q. Li, R. Qiao, L.A. Wray, J. Chen, Z. Zhuo, Y. Chen, S. Yan, F. Pan, Z. Hussain, W. Yang, J. Phys. D Appl. Phys., 49 (2016) 413003.
[52] R. Qiao, T. Chin, S.J. Harris, S. Yan, W. Yang, Curr. Appl. Phys., 13 (2013) 544-548.
[53] Z. Zhuo, P. Olalde-Velasco, T. Chin, V. Battaglia, S.J. Harris, F. Pan, W. Yang, Appl. Phys. Lett., 110 (2017) 093902.
[54] X. Liu, J. Liu, R. Qiao, Y. Yu, H. Li, L. Suo, Y.-s. Hu, Y.-D. Chuang, G. Shu, F. Chou, T.-C. Weng, D. Nordlund, D. Sokaras, Y.J. Wang, H. Lin, B. Barbiellini, A. Bansil, X. Song, Z. Liu, S. Yan, G. Liu, S. Qjao, T.J. Richardson, D. Prendergast, Z. Hussain, F.M.F. de Groot, W. Yang, J. Am. Chem. Soc., 134 (2012) 13708-13715.
[55] R. Qiao, L.A. Wray, J.-H. Kim, N.P.W. Pieczonka, S.J. Harris, W. Yang, J. Phys. Chem. C, 119 (2015) 27228-27233.
[56] J. Zheng, G. Teng, C. Xin, Z. Zhuo, J. Liu, Q. Li, Z. Hu, M. Xu, S. Yan, W. Yang, F. Pan, J. Phys. Chem. Lett., 8 (2017) 5537-5542.
[57] R. Qiao, J. Liu, K. Kourtakis, M.G. Roelofs, D.L. Peterson, J.P. Duff, D.T. Deibler, L.A. Wray, W. Yang, J. Power Sources, 360 (2017) 294-300.
[58] R. Qiao, K. Dai, J. Mao, T.-C. Weng, D. Sokaras, D. Nordlund, X. Song, V.S. Battaglia, Z. Hussain, G. Liu, W. Yang, Nano Energy, 16 (2015) 186-195.
[59] A.J. Achkar, T.Z. Regier, E.J. Monkman, K.M. Shen, D.G. Hawthorn, Sci Rep, 1 (2011) 182.
[60] R. Qiao, L.A. Wray, J.-H. Kim, N.P.W. Pieczonka, S.J. Harris, W. Yang, The Journal of Physical Chemistry C, 119 (2015) 27228-27233.
[61] A. Firouzi, R. Qiao, S. Motallebi, C.W. Valencia, H.S. Israel, M. Fujimoto, L.A. Wray, Y.D. Chuang, W. Yang, C.D. Wessells, Nat. Commun., 9 (2018) 861.
[62] W. Manchot, H. Gall, Berichte der deutschen chemischen Gesellschaft (A and B Series) B, 61 (1928) 1135-1140.
[63] L. Wang, J. Song, R. Qiao, L.A. Wray, M.A. Hossain, Y.D. Chuang, W. Yang, Y. Lu, D. Evans, J.J. Lee, S. Vail, X. Zhao, M. Nishijima, S. Kakimoto, J.B. Goodenough, J. Am. Chem. Soc., 137 (2015) 2548-2554.
[64] M. Pasta, R.Y. Wang, R. Ruffo, R. Qiao, H.-W. Lee, B. Shyam, M. Guo, Y. Wang, L.A. Wray, W. Yang, M.F. Toney, Y. Cui, J. Mater. Chem. A, 4 (2016) 4211-4223.
[65] J. Wu, J. Song, K. Dai, Z. Zhuo, L.A. Wray, G. Liu, Z.X. Shen, R. Zeng, Y. Lu, W. Yang, J. Am. Chem. Soc., 139 (2017) 18358-18364.
[66] F.M.F. de Groot, M. Grioni, J.C. Fuggle, J. Ghijsen, G.A. Sawatzky, H. Petersen, Phys. Rev. B, 40 (1989) 5715-5723.
[67] A. Augustsson, G.V. Zhuang, S.M. Butorin, J.M. Osorio-Guillen, C.L. Dong, R. Ahuja, C.L. Chang, P.N. Ross, J. Nordgren, J.-H. Guo, The Journal of Chemical Physics, 123 (2005) 184717.
[68] H.M. Hollmark, T. Gustafsson, K. Edstrom, L.C. Duda, Phys. Chem. Chem. Phys., 13 (2011) 20215-20222.
[69] W.-S. Yoon, M. Balasubramanian, K.Y. Chung, X.-Q. Yang, J. McBreen, C.P. Grey, D.A. Fischer, J. Am. Chem. Soc., 127 (2005) 17479-17487.
[70] M.G. Kim, H.J. Shin, J.-H. Kim, S.-H. Park, Y.-K. Sun, J. Electrochem. Soc., 152 (2005) A1320-A1328.

[71] J. Zhou, D. Hong, J. Wang, Y. Hu, X. Xie, H. Fang, Phys. Chem. Chem. Phys., 16 (2014) 13838-13842.
[72] E. Yilmaz, C. Yogi, K. Yamanaka, T. Ohta, H.R. Byon, Nano Lett., 13 (2013) 4679-4684.
[73] R. Qiao, Y.D. Chuang, S. Yan, W. Yang, PLoS One, 7 (2012) e49182.
[74] P. Glans, K. Gunnelin, P. Skytt, J. Guo, N. Wassdahl, J. Nordgren, H. Agren, F.K. Gel'mukhanov, T. Warwick, E. Rotenberg, Phys. Rev. Lett., 76 (1996) 2448-2451.
[75] M. Oishi, T. Fujimoto, Y. Takanashi, Y. Orikasa, A. Kawamura, T. Ina, H. Yamashige, D. Takamatsu, K. Sato, H. Murayama, H. Tanida, H. Arai, H. Ishii, C. Yogi, I. Watanabe, T. Ohta, A. Mineshige, Y. Uchimoto, Z. Ogumi, J. Power Sources, 222 (2013) 45-51.
[76] M. Oishi, C. Yogi, I. Watanabe, T. Ohta, Y. Orikasa, Y. Uchimoto, Z. Ogumi, J. Power Sources, 276 (2015) 89-94.
[77] N. Yabuuchi, M. Nakayama, M. Takeuchi, S. Komaba, Y. Hashimoto, T. Mukai, H. Shiiba, K. Sato, Y. Kobayashi, A. Nakao, M. Yonemura, K. Yamanaka, K. Mitsuhara, T. Ohta, Nat. Commun., 7 (2016) 13814.
[78] W.E. Gent, K. Lim, Y. Liang, Q. Li, T. Barnes, S.J. Ahn, K.H. Stone, M. McIntire, J. Hong, J.H. Song, Y. Li, A. Mehta, S. Ermon, T. Tyliszczak, D. Kilcoyne, D. Vine, J.H. Park, S.K. Doo, M.F. Toney, W. Yang, D. Prendergast, W.C. Chueh, Nat. Commun., 8 (2017) 2091.
[79] J. Xu, M. Sun, R. Qiao, S.E. Renfrew, L. Ma, T. Wu, S. Hwang, D. Nordlund, D. Su, K. Amine, J. Lu, B.D. McCloskey, W. Yang, W. Tong, Nat. Commun., 9 (2018) 947.
[80] S.M. Butorin, J. Guo, N. Wassdahl, E.J. Nordgren, J. Electron. Spectrosc. Relat. Phenom., 110-111 (2000) 235-273.
[81] J. Guo, J. Electron. Spectrosc. Relat. Phenom., 188 (2013) 71-78.
[82] P.P.R.M.L. Harks, F.M. Mulder, P.H.L. Notten, J. Power Sources, 288 (2015) 92-105.
[83] L. Weinhardt, M. Blum, O. Fuchs, A. Benkert, F. Meyer, M. Bär, J.D. Denlinger, W. Yang, F. Reinert, C. Heske, J. Electron. Spectrosc. Relat. Phenom., 188 (2013) 111-120.
[84] A. Benkert, M. Blum, F. Meyer, R.G. Wilks, W. Yang, M. Bar, F. Reinert, C. Heske, L. Weinhardt, Rev. Sci. Instrum., 85 (2014) 015119 (015115 pp.)-015119 (015115 pp.).
[85] M. Blum, L. Weinhardt, O. Fuchs, M. Bar, Y. Zhang, M. Weigand, S. Krause, S. Pookpanratana, T. Hofmann, W. Yang, J.D. Denlinger, E. Umbach, C. Heske, Rev. Sci. Instrum., 80 (2009) 123102.
[86] X. Liu, W. Yang, Z. Liu, Adv. Mater., 26 (2014) 7710-7729.